

# Characterization of the field-effect addressable potentiometric sensor (FAPS)

S. Böhm, W.J. Parak, M. George, H.E. Gaub, A. Lorke\*

*Sektion Physik and Center for Nano Science (CENS), Ludwig Maximilians Universität (LMU)-München, Geschwister-Scholl-Platz 1, 80539 München, Germany*

## Abstract

The field-effect addressable potentiometric sensor (FAPS) is a surface potential sensor with the option of high spatial resolution. It is based on the ability to control the resistance of field-effect channels in thin semiconductor films with electrical potentials. Compared to arrays of standard field-effect transistors (FET), the number of required leads is drastically reduced by arranging the field-effect channels and underlying gate electrodes in a grid structure. In order to investigate the practicability of the physical concept, a test structure was built by using the epitaxial lift-off technique. It was demonstrated that the concept of the FAPS can be put into practice. The frequency dependence of the test structure was analyzed experimentally and theoretically. At a time resolution of 3 kHz, the potential sensitivity was found to be better than 150  $\mu\text{V}$ . © 2000 Elsevier Science S.A. All rights reserved.

*Keywords:* Surface potential sensor; Potential sensitivity; Field-effect addressable potentiometric sensor; FAPS; Epitaxial lift-off

## 1. Introduction

Surface potential sensors are the basis of many instruments for chemical imaging. In order to monitor several substances in parallel or to obtain the spatial distribution of one substance, spatial resolution is required [1,2]. The option of spatial resolution of surface potential sensors with discrete sites is determined by (i) the number of addressable sites, (ii) the diameter of one site and (iii) the separation between adjacent sites. In practice, however, these parameters are strongly correlated. One major problem to design devices with a high integration density of addressable points is the arrangement of the electrical connectors. In arrays of field-effect transistors (FET) [3–7], each site, i.e. each gate electrode, needs to be connected by at least one individual lead.

Like FETs, the field-effect addressable potentiometric sensor (FAPS) is based on the possibility to tune the local resistance of a field-effect channel by applying a bias voltage with a gate (G) electrode to the channel [8]. In standard FETs, the resistance of a field-effect channel that is connected by two terminals — drain (D) and source (S)

— is usually measured by recording the drain-source current at constant drain-source voltage. If the bias voltage is set to the working point, where small potential variations lead to big changes in the resistance, variations in surface potential can be detected by measuring the corresponding changes in resistance. In contrast to arrays of FETs, the FAPS is built as a grid structure of perpendicular field-effect channels and gate electrodes, which are located below the field-effect channels. This grid structure allows for a connecting scheme that scales only with the square root of the number of addressable sites. Here, the sites are defined as intersections of the field-effect channels and the gate electrodes. The procedure of addressing individual sites has recently been described in greater detail [8].

The aim of this study is to demonstrate that the recently proposed concept of the FAPS can be put into practice. For this purpose, a device with field-effect channels that were based on a quantum-well heterostructure was developed and its basic characteristics were investigated. In quantum wells, free electrons are trapped as a 2-dimensional electron gas, whose local density can be reduced by applying negative voltages [9]. One key parameter of such surface potential detectors is their potential sensitivity at a certain time resolution.

A possible application of the FAPS is the development of cell-semiconductor-hybrids [8]. The idea is to record

\* Corresponding author.: Tel.: +49-89-2180-3732; fax: +49-89-2180-3182.

*E-mail address:* axel.lorke@physik.uni-muenchen.de (A. Lorke).

changes in the electric, extracellular potential of living cells with a surface potential detector [10–12]. For such applications, a potential sensitivity of about  $100 \mu\text{V}$  at a time resolution of 3 kHz is required. Therefore, in this study, the potential sensitivity of the FAPS will be determined at a time resolution of 3 kHz.

## 2. Materials and methods

As test structure, a device consisting of five field-effect channels and one gate electrode below the field-effect channels and thus five addressable sites was built. The device is based on a AlGaAs/InGaAs/AlGaAs heterostructure that has been grown by molecular beam epitaxy on top of a GaAs substrate (Siemens, München, Germany). Between the GaAs substrate and the heterostructure, a sacrificial layer of 50 nm AlAs was inserted during the manufacturing process. The heterostructure had a thickness of  $\approx 500 \text{ nm}$  and the layer sequence is shown in detail in Fig. 1. Within this heterostructure, the actual n-type field-effect channel consisted of a 12-nm-thick InGaAs layer. With the technique of the so-called epitaxial lift-off [13], the AlGaAs/InGaAs/AlGaAs heterostructure could be peeled off from its GaAs substrate by etching the sacrificial layer with hydrofluoric acid. The so-separated heterostructure could be put on top of a designated surface and adhered there due to van der Waals interaction [14].

In the first step of the fabrication, a  $\approx 100\text{-nm}$ -thick NiCr layer was deposited on top of a glass substrate. By using standard lithographic techniques [15], one gate electrode was defined, see Fig. 2. Next, the AlGaAs/

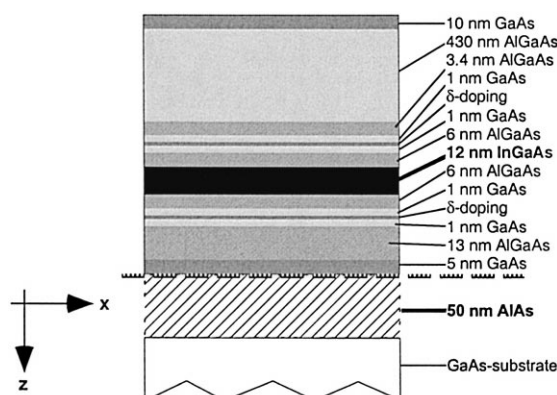


Fig. 1. Layer sequence of the AlGaAs/InGaAs/AlGaAs-heterostructure, not drawn to scale. The total thickness of the epitaxially grown heterostructure was  $\approx 500 \text{ nm}$ . The actual field-effect channel consisted of a 12-nm-thick InGaAs layer that is drawn in black. Together with the two surrounding AlGaAs layers, a quantum well structure is formed. The n-type quantum well was filled with electrons from two  $\delta$ -doping layers. An AlAs sacrificial layer was grown directly upon the GaAs substrate. By etching the AlAs layer, the heterostructure could be peeled off from its GaAs substrate. The supplemental layers between the AlAs and the quantum well were inserted to adopt the lattice constants of both layers and thus ensured a homogeneous crystal growth. The supplemental layers above the quantum well were grown as cap.

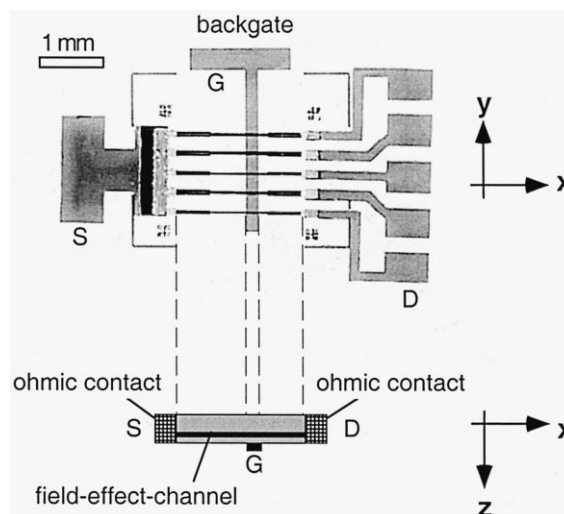


Fig. 2. Top view and cross-section of the FAPS test structure. The scale bar in the top view represents 1 mm, the cross-section through one field-effect channel is not drawn to scale. The test structure consisted of five parallel field-effect channels, which were built from the AlGaAs/InGaAs/AlGaAs layer structure shown in Fig. 1, and one backgate electrode. Analogous to FETs, the three terminals are called source (S), gate (G) and drain (D).

InGaAs/AlGaAs heterostructure was prepatterned with Ohmic contacts, epitaxially lift-off from its GaAs substrate and deposited on the surface of the glass substrate on top of the gate electrode. By using standard lithographic techniques and a chemical wet-etching process, the heterostructure was patterned in five field-effect channels. Finally, metallic leads were deposited to electrically connect the gate electrode and the five field-effect channels. In Fig. 2, the arrangement of the backgate electrode below the field-effect channels and a schematic cross-section through one field-effect channel is shown. The total length and width of the field-effect channels was 2 mm and  $65 \mu\text{m}$ , respectively. The width of the backgate electrode was  $200 \mu\text{m}$ .

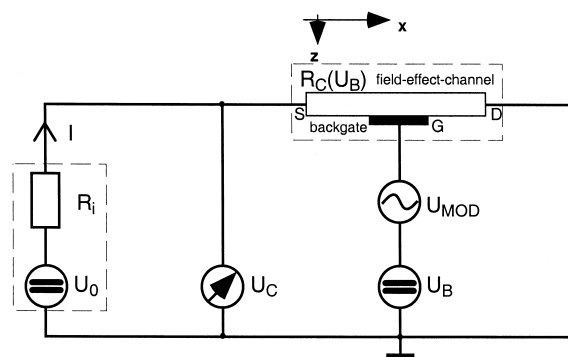


Fig. 3. Scheme of the electric setup, which was used for the characterization measurements. A current  $I$  was injected in one field-effect channel with a current source with inner resistance  $R_i$  and electromotive force  $U_0$ , and the voltage drop  $U_C$  along the channel was measured with a voltmeter with high input resistance. A (DC) bias voltage  $U_B$  was applied to the backgate electrode. For frequency-dependent measurements, an AC modulation  $U_{\text{MOD}}$  was added to the bias.

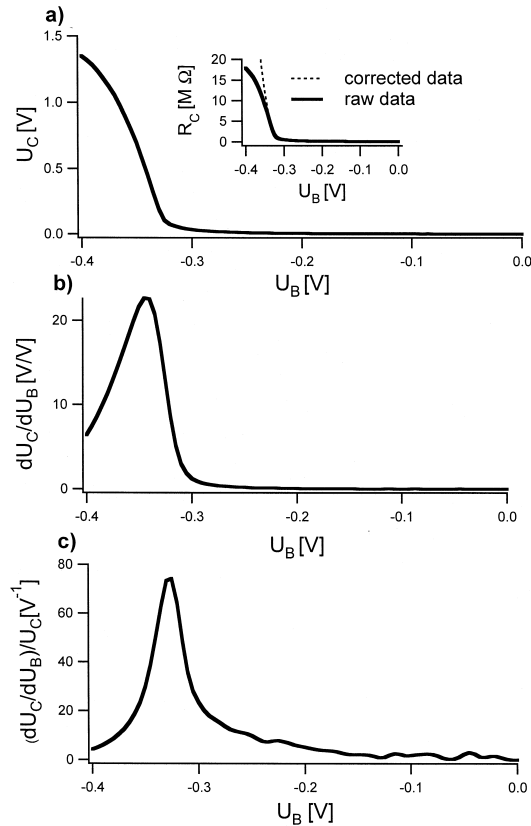


Fig. 4. (a) Quasi-static transfer characteristics  $U_C(U_B)$  of the FAPS test structure. The voltage drop  $U_C$  along the field-effect channel is plotted vs. the bias voltage  $U_B$ . The bend in the  $U_C(U_B)$  characteristics at bias voltages  $\lesssim -0.35$  V was caused by the finite resistance  $R_i$  of the current source and is not due to a decrease in the channel resistance. The insert shows the calculated corresponding resistance of the field-effect channel  $R_C$ . The solid line was obtained assuming a voltage-independent current  $I$  and, thus, multiplying the raw data with  $R_i/U_0$ :  $R_C(\text{raw data}) = U_C R_i / U_0$ . In order to compensate for the finite size of the inner resistance of the current source, the voltage dependence of the current  $I = I(U_C)$  was taken into account:  $R_C(\text{corrected data}) = U_C R_i / (U_0 - U_C)$ . For further correction, the finite inner resistance of the voltmeter that was employed to measure  $U_C$  would have to be taken into account. Both curves match besides (very) negative bias voltages. (b) Slope of the transfer characteristics  $dU_C/dU_B$ , derived by differentiation of the data shown in (a). It is maximum at the bias voltage at which the resistance of the field-effect channel was increased to the same order of magnitude as the inner resistance. (c) Normalized slope  $S = (dU_C/dU_B)/U_C$ , calculated by dividing the data shown in (b) and (a).

In Fig. 3, the scheme of the electric circuit is shown that has been used for the characterization measurements. All measurements, if not stated otherwise, were performed at room temperature under dark conditions in a shielded copper box. A constant current  $I \approx 0.75 \mu\text{A}$  was injected in one field-effect channel. Since the control rate of the current source had to be very fast to investigate the frequency dependence of the FAPS device, a battery  $U_0$  with a resistance  $R_i = 20 \text{ M}\Omega$  in series was used for this purpose.

In order to determine the transfer characteristics of the device, i.e. the voltage dependency of the resistance of the field-effect channel  $R_C(U_B)$ , a bias (DC) voltage  $U_B$  was

applied to the backgate electrode and the voltage drop  $U_C(U_B) = R_C I$  along the field-effect channel was measured, see Fig. 4a.  $U_C$  was recorded with a voltage amplifier with high input resistance ( $> 100 \text{ M}\Omega$ ). Since the  $U_C(U_B)$  curves were sometimes found to shift along the  $U_B$ -axis on the time scale of minutes, this shift was compensated in all figures shown in this study. The noise  $\delta U_C$  in the  $U_C$  measurements was determined in a parallel experiment. For several bias voltages  $U_B$ , the resulting  $U_C$  signal was filtered with a 0.03 Hz high-pass filter for offset compensation, and a 3 kHz low-pass filter. Fluctuations  $\Delta U_C(t)$  were then recorded with a sampling frequency of 10 kHz. Finally, the noise level  $\delta U_C$  was defined as the mean width of the voltage fluctuation  $\Delta U$  over a period of 1 s, see Fig. 5a. The corresponding noise level in the determination of the resistance of the field-effect channel  $\delta R_C$  is given by  $\delta U_C = \delta R_C I$ .

Two characteristic numbers were derived from these data. The normalized slope  $S = (dU_C/dU_B)/U_C = (dR_C/dU_B)/R_C$  is a measure for the steepness of the

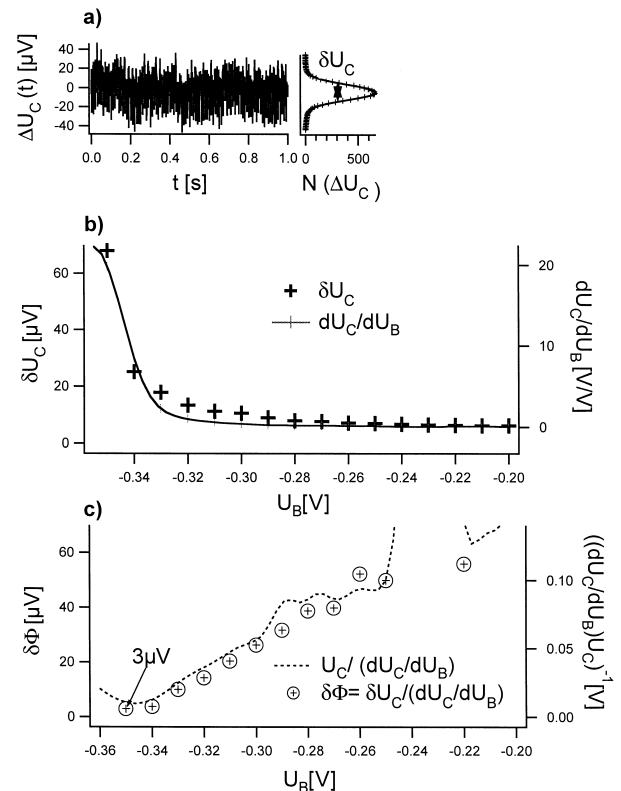


Fig. 5. (a) Fluctuation  $\Delta U_C(t)$ , recorded after offset compensation and a 3 kHz low-pass filter with a sampling rate of 10 kHz at fixed bias voltage  $U_B = -0.35$  V. Within 1 s, 10,000 data points were recorded. The histogram  $N(\Delta U_C)$  shows the distribution of the data points. The noise level  $\delta U_C$  was defined as the mean width of the Gaussian distribution. (b) Noise level  $\delta U_C(U_B)$ , determined at several bias voltages  $U_B$  (left axis). In the same diagram, the slope of the transfer characteristics  $dU_C/dU_B$  is shown (right axis, data points analogues to Fig. 4b). (c) Potential sensitivity  $\delta\Phi = \delta U_C / (dU_C/dU_B)$  and reciprocal normalized slope  $S^{-1} = U_C / (dU_C/dU_B)$ , calculated by using the data points shown in Figs. 4a,b, 5b.

slope of the resistance–voltage characteristics [8]. Since the unit of  $S$  is reciprocal Volt, numbers obtained with the FAPS can be compared to numbers obtained with competitive devices, like FETs. In this study, the voltage sensitivity  $\delta\Phi$  of the FAPS is defined as noise level in surface potential measurements:  $\delta\Phi = \delta U_C / (dU_C/dU_B) = \delta R_C / (dR_C/dU_B)$ , see Fig. 5c. The smaller  $\delta\Phi$ , the better the voltage sensitivity is.

To characterize the frequency dependence of the slope of the transfer characteristics  $dU_C/dU_B$ , a small modulation (AC) voltage  $U_{MOD}$  with an amplitude of  $\approx 1$  mV and a frequency  $f_{MOD}$  was added to the (DC) bias voltage  $U_B$ . The amplitude of the bias voltage  $U_B$  was applied as a ramp with a slow sweep velocity of 30 mV/s, and the amplitude of the resulting modulation of  $U_C$ , i.e. the amplitude of the AC part of the  $U_C$  signal, was measured using a lock-in amplifier. This amplitude is directly equivalent to the slope of the transfer characteristics  $dU_C/dU_B$  ( $f_{MOD}$ ), see Fig. 6a.

In all experiments described so far, the potentials acting on the field-effect channel were applied from below, i.e. by using a backgate electrode. However, the concept of the FAPS of measuring surface potentials is based on the idea that the electric fields generated by potentials applied from above and below the channel add. To demonstrate the sensitivity of the channel resistance on voltages applied from both sides, the following experiment was performed. A frontgate electrode was added to a test structure similar

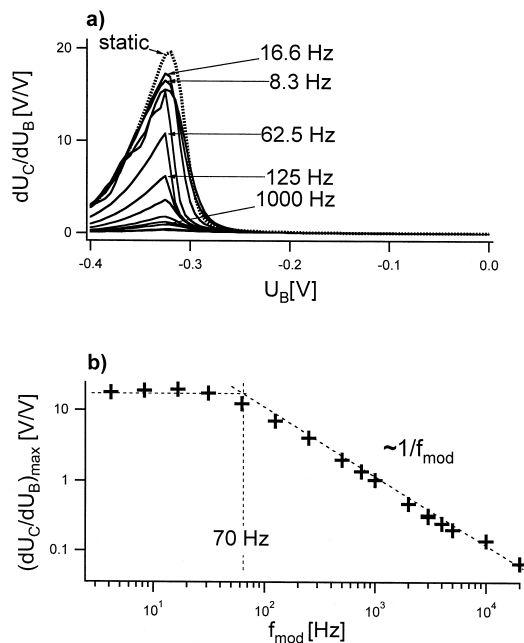


Fig. 6. (a) Frequency dependence of the dynamic slope  $dU_C/dU_B$ , obtained by adding an AC modulation with frequency  $f_{MOD}$  to the bias voltage and detecting the AC response in  $U_C$  with a lock-in amplifier.  $dU_C/dU_B$  is shown for several modulation frequencies. The dotted curve describes the (quasi-) static slope that has been shown in Fig. 4b. (b) Maximum of the slope for several frequencies (see (a)), plotted vs. the modulation frequency  $f_{MOD}$ . For low frequencies, the slope is almost constant, whereas it decays  $\propto 1/f_{MOD}$  for high frequencies.

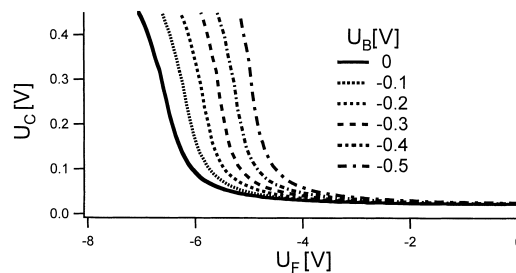


Fig. 7. Quasi-static transfer characteristics  $U_C(U_F)$  of the FAPS test structure with an additional frontgate electrode. The voltage drop  $U_C$  along the field-effect channel is plotted vs. the bias voltage  $U_F$  applied to the frontgate. The bias voltage  $U_B$  applied to the backgate was held constant.

to the one described above by depositing a  $\approx 100$ -nm-thick NiCr layer on top of the test structure and using standard lithographic techniques. The effective width of the frontgate was  $\approx 600$   $\mu\text{m}$ . A constant current  $I \approx 0.7$   $\mu\text{A}$  was injected in one field-effect channel. Subsequently, several constant (DC) bias voltages  $U_B$  were applied to the backgate. For each value of  $U_B$ , the transfer characteristic  $U_C(U_F)$  of the device was determined by biasing the frontgate with a (DC) voltage  $U_F$  and recording the corresponding voltage drop  $U_C(U_F) = R_C I$  along the field-effect channel, see Fig. 7. The experimental setup for measuring  $U_C$  was analogous to the one described in Fig. 3. The electron density in the channel was increased as a result of constant illumination of the test structure with a standard microscope light source.

### 3. Results

A typical transfer characteristics  $U_C(U_B)$  of the test structure is shown in Fig. 4a. It is obvious that the voltage drop along the channel  $U_C$  and, therefore, the resistance of the channel  $R_C$  is steeply raised for negative bias voltages  $U_B$ , whereas it was almost constant for voltages around zero and positive bias. The slope of the transfer characteristics  $dU_C/dU_B$  describes how much the voltage drop along the field-effect channel is changed by a certain variation in the applied potential, see Fig. 4b. With the described electric setup, normalized slopes of the transfer characteristics  $S = (dU_C/dU_B)/U_C$  up to  $\approx 70$   $\text{V}^{-1}$  were achieved, see Fig. 4c.

In Fig. 5a and b, the noise  $\delta U_C$  in measuring  $U_C$  is shown.  $\delta U_C$  was found to increase at negative bias voltages and, thus, showed a similar behavior as the slope of the transfer characteristics  $dU_C/dU_B$ , although  $\delta U_C$  rose less steep than  $dU_C/dU_B$ . The obtained results for the potential sensitivity of the FAPS  $\delta\Phi = \delta U_C / (dU_C/dU_B)$  are depicted in Fig. 5c. They were derived from the noise in  $U_C$ -measurements  $\delta U_C$ , which was scaled with the slope of the transfer characteristics  $dU_C/dU_B$ .  $\delta\Phi$  was found to be approximately linear to the applied bias voltage. This means that the better the potential sensitivity is, the more

the channel is depleted of free electrons. The same behavior was found for the reciprocal normalized slope  $S^{-1}$ , see Fig. 5c.

The task of any surface potential sensor like the FAPS is to record changes in the potential located at the surface of the device. With the FAPS, changes in the potential are recorded as changes in the resistance or in the corresponding voltage drop along the field-effect channel. In Fig. 6, it is shown that the slope of the transfer characteristics of the FAPS depends on the frequency of the potential variation. With increasing modulation frequency  $f_{\text{MOD}}$ ,  $dU_C/dU_B$  was found to decrease.  $dU_C/dU_B$  describes how much  $U_C$  is changed by a certain potential variation this result involves, i.e. fast potential variations change the resistance of the field-effect channel less than quasi-static ones. Therefore, the potential sensitivity of the FAPS depends on the time resolution. For high frequencies  $\geq 70$  Hz, the slope of the transfer characteristics  $dU_C/dU_B$  at the working point was found to decay proportional to the reciprocal frequency, see Fig. 6b.

By using a 3 kHz low-pass filter, the noise in  $U_C$  measurements at the working point ( $U_B \approx -0.35$  V) was found to be  $\delta U_C \approx 65$   $\mu\text{V}$ , see Fig. 5b. The quasi-static slope of the transfer characteristics was  $dU_C/dU_B \approx 22$ , see Figs. 5b and 6, whereas the slope at a modulation frequency of 3 kHz was  $dU_C/dU_B \approx 0.4$ , see Fig. 6. Therefore, the potential sensitivity of the FAPS test structure described in this study at a time resolution of 3 kHz is  $\delta\Phi = 65$   $\mu\text{V}/0.4 \approx 150$   $\mu\text{V}$ . However, the sensitivity to detect quasi-static signals is at least  $\delta\Phi = 65$   $\mu\text{V}/22 \approx 3$   $\mu\text{V}$ , since further filtering should significantly lower  $\delta U_C$ .

When the field-effect channel was biased both from above and below by applying potentials with a frontgate and backgate electrode, its resistance depended on the resulting electric field caused by both potentials. This can be seen from the data shown in Fig. 7, where a constant additional voltage  $U_B$  applied to the backgate shifted the transfer characteristics  $U_C(U_F)$ , i.e. the dependence of the channel resistance ( $\propto U_C$ ) on the potential  $U_F$  applied to the frontgate, parallel to the voltage axis. The shape of each  $U_C(U_F)$  curve shown in Fig. 7 is very similar to the shape of the  $U_C(U_B)$  curve shown in Fig. 4a, although the onset of the depletion of the channel and, therefore, the working point was shifted to more negative bias voltages ( $U_B \approx -0.35$  V in Fig. 4a compared to  $U_F \approx -6$  V in Fig. 7) and the slope of the transfer-characteristics was smaller.

#### 4. Discussion

In this study, a test structure was developed and characterized to demonstrate that the concept of the FAPS is realizable. It has been shown that by changing the bias voltage that was applied to the backgate electrode located under a field-effect channel, the resistance of the channel could be controlled. Since the transfer characteristics of the test structure ( $R_C(U_B)$ ,  $U_C(U_B)$ ) was found to be highly

nonlinear, it is possible to apply bias voltages, where the resistance of the field-effect channel is nearly independent of changes in the electric potential ( $|dR_C/dU_B| \rightarrow 0$ ,  $|dU_C/dU_B| \rightarrow 0$ ), as well as it is possible to bias the device, so that potential variations strongly change the resistance ( $|dR_C/dU_B| \gg 0$ ,  $|dU_C/dU_B| \gg 0$ ). This suggests that indeed field-effect channels, which fulfill the demands of the FAPS concept [8], can be constructed on the basis of a AlGaAs/InGaAs/AlGaAs heterostructure.

At this point, the experimental setup for the resistance measurements has to be discussed. If the current through the field-effect channel is in the first order, assumed to be  $I = U_0/R_i$  and, therefore, independent of the applied bias  $U_B$ , then the resistance  $R_C$  of the field-effect channel is directly linear to the measured voltage drop  $U_C$ . However, this assumption is certainly only valid, if the total resistance of the field-effect channel  $R_C$  is significantly smaller than the inner resistance of the current source  $R_i$  (20 M $\Omega$ ). For positive bias voltages  $U_B$  and bias voltages around zero, the resistance of the field-effect channel was found to be  $\approx 100$  k $\Omega$  and was, thus, significantly smaller than  $R_i$ . In contrast, for more negative voltages  $U_B$ , the resistance of the field-effect channel rose to values higher than 20 M $\Omega$ . Due to the effect of a voltage divider, here the current  $I$  became smaller than  $U_0/R_i$  and, therefore,  $I$  can no longer be assumed to be constant. In this region, a voltage-dependent current  $I(U_B) = U_0/(R_i + R_C(U_B))$  has to be assumed, as can be seen from the equivalent circuit depicted in Fig. 3. In Fig. 4a, both the raw data, where a constant current was assumed ( $R_C = U_C R_i/U_0$ ), and the corrected data, where the voltage dependence of the current was taken into account ( $R_C = U_C R_i/(U_0 - U_C)$ ), are shown. Both curves match, besides negative voltages  $\lesssim -0.3$  V. The transfer characteristics  $R_C(U_B)$  drawn with the corrected data has a hyperbolic shape, which was predicted for a n-type field-effect channel [8]. Measurements were additionally limited by the input resistance of the voltmeter ( $\approx 100$  M $\Omega$ ), which was employed to detect  $U_C$ . For negative bias voltages, when the resistance of the field-effect channel rose to values in the range of 100 M $\Omega$ , current flow into the voltmeter needs to be considered. Again this effect involves that the current  $I$  becomes smaller than  $U_0/(R_i + R_C(U_C))$ . To avoid a correction of the raw data that would involve two steps to compensate for the finite inner resistance of the current source  $R_i \ll \infty$  and for the finite resistance of the voltmeter, besides Fig. 4a, only raw data  $U_C$  are presented in this study and a transformation into  $R_C$  was omitted. The shown slope of the transfer characteristics  $U_C(U_B)$  has its maximum at a bias voltage, where the resistance of the field-effect channel reaches the same order of magnitude as  $R_i$ , and decreases for more negative voltages, see Fig. 4b. This maximum in the measured voltage drop  $U_C$ , therefore, does not result from a maximum in the resistance of the field-effect channel  $R_C$ , but has to be considered as an artifact due to the electric detection scheme.  $R_C$  is ex-

pected to further increase upon applying more negative bias voltages. However, the simplification of using  $U_C$  instead of  $R_C$  does not involve any loss in the physical description of the device.

Comparison of Figs. 4a and 7 shows that the  $U_C(U_B)$  and  $U_C(U_F)$  characteristics are very similar, i.e. bias potentials can be applied comparably from both below and above the field-effect channel. However, for the reason of availability, an asymmetric heterostructure was used in this study. As can be seen in Figs. 1 and 2, the closest possible distance between the InGaAs field-effect channel and a backgate and frontgate electrode is 20 and 450 nm, respectively, simply given by the thickness of the GaAs and AlGaAs spacer layers. Therefore, the electric field acting on the field-effect channel due to a bias voltage  $U_F$  applied to the frontgate is about 20 times lower than the respective field caused by a potential  $U_B$  of the backgate electrode. This explains that in the case of employing the frontgate the onset of the depletion of the channel is shifted to much more negative bias voltages ( $U_F \approx -6 \text{ V} = 20(-0.3 \text{ V})$  in Fig. 7 compared to  $U_B \approx -0.35 \text{ V}$  in Fig. 4a) and  $|dU_C(U_F)/dU_F| \ll |dU_C(U_B)/dU_B|$ . For an optimized surface potential sensor, a structure has to be used in which the InGaAs field-effect channel is closer to the front surface of the device in order to increase surface potential sensitivity. Additional differences between the  $U_C(U_B)$  curve shown in Fig. 4a and the  $U_C(U_F)$  curve shown in Fig. 7 may have been caused because the width of the backgate and frontgate electrode was different and because the test structure with the frontgate was illuminated and was fabricated from a different semiconductor wafer.

The data presented in Fig. 7 further demonstrate that the sensitivity of a potential  $U_F$  applied to the front surface on the field-effect channel can be tuned by applying a bias potential  $U_B$  at the back surface. That is, the transfer characteristics  $U_C(U_F)$  and therewith the sensitivity of potentials located on the front surface of the device on the channel resistance can be controlled by steering the potential  $U_B$  of the backgate electrode.

As shown in Fig. 5b, the noise in  $U_C$  measurements  $\delta U_C$  rose slower with negative bias voltages  $U_B$  than the slope of the quasi-static transfer characteristics. This involves that  $\delta\Phi = \delta U_C / (dU_C/dU_B)$  depends on the applied bias and is smaller for negative voltages  $U_B$ , see Fig. 5c. Therefore, the potential sensitivity is best at negative bias voltages, where the slope of the  $U_C(U_B)$  curve is maximum, and here the working point of the device should be selected. The shape of the reciprocal normalized slope  $S^{-1}(U_B) = U_C / (U_C/dU_B)$  corresponds to the shape of the  $\delta\Phi(U_B)$  curve for quasi-static measurements, see Fig. 5c. This indicates that the normalized slope is a reasonable parameter for comparing the potential sensitivity of the FAPS and other surface potential detectors. In contrast to determine  $\delta\Phi(U_B)$ , which requires two independent measurements ( $U_C(U_B)$  and  $\delta U_C(U_B)$ ),  $S^{-1}$  can be determined by just one measurement ( $U_C(U_B)$ ).

The slope of the transfer characteristics was found to decrease with the modulation frequency of the applied bias potential, see Fig. 6. This can be explained by assuming the field-effect channel as a series of resistors, and by describing the junction between the gate electrode and the field-effect channel as capacitor  $C$ , as shown in the small-signal equivalent circuit in Fig. 8. At a modulation frequency  $\omega_{\text{MOD}} = 2\pi f_{\text{MOD}}$ , only a fraction of the applied modulation voltage  $U_{\text{MOD}}$  causes an electric field perpendicular to the field-effect channel. This fraction, the effective modulation potential  $U_{\text{MOD,eff}}$ , is given by the law of a voltage divider:  $U_{\text{MOD,eff}} = U_{\text{MOD}}(i\omega_{\text{MOD}}C)^{-1} / (R + (i\omega_{\text{MOD}}C)^{-1}) = U_{\text{MOD}} / (1 + (\omega_{\text{MOD}}RC)^{-1})$ , where  $R$  is the Ohmic resistance of both sides of the field-effect channel and  $(i\omega_{\text{MOD}}C)^{-1}$  is the impedance of the gate electrode/field-effect channel junction, see Fig. 8. Under quasi-static conditions ( $\omega_{\text{MOD}} \rightarrow 0$ ), the impedance of the capacitance  $(i\omega_{\text{MOD}}C)^{-1}$  is infinite, and all applied voltage  $U_{\text{MOD}}$  drops at the junction between the gate and the field-effect channel ( $U_{\text{MOD,eff}} \rightarrow U_{\text{MOD}}$ ). For high frequencies ( $\omega_{\text{MOD}} \gg RC$ ), the impedance of the capacitor is reduced and a significant fraction of the modulation voltage drops along the field-effect channel and does not contribute to the electric field perpendicular to the channel. Therefore, the effective modulation potential  $U_{\text{MOD,eff}}$  is reduced and decreases proportional to  $1/f_{\text{MOD}}$ . The amplitude of the effective modulation potential is directly correlated to the slope of the transfer characteristics  $dU_C/dU_B(\omega_{\text{MOD}})$ , see Fig. 6b. The decline in the slope of the transfer characteristics starts, as the modulation frequency reaches the order of  $RC$ . In this study, quasi-static behavior has been observed for modulation frequencies  $f_{\text{MOD}} \lesssim 70 \text{ Hz}$ ; whereas for higher modulation frequencies, the slope of the transfer characteristics was reduced  $\propto 1/f_{\text{MOD}}$ .

The transition frequency can be estimated if the geometry of the test structure is known. The capacitance  $C$  can be calculated by assuming the junction between the gate electrode and the field-effect channel as a plane capacitor  $C = \epsilon_0 \epsilon_C A/d$ . In the test structure that has been described in this study, the distance  $d$  between the gate

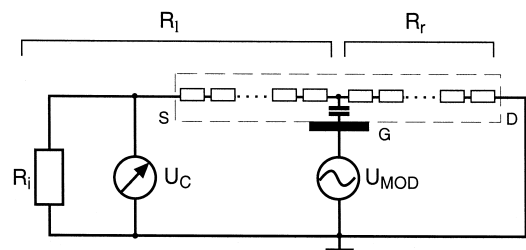


Fig. 8. Small-signal equivalent circuit. All constant voltage and current sources ( $U_0$ ,  $U_B$ ) are removed. The field-effect channel is described as a series of resistors and the junction between the channel and the gate as a capacitor  $C$ . The resistance  $R$  is a parallel circuit of  $R_l$  and  $R_r$ , where  $R_l$  and  $R_r$  are the resistance on the left and right sides of the field-effect channel, respectively.

electrode and the field-effect channel was  $\approx 26$  nm, see Fig. 1. The area  $A$  of the intersection between the gate and the channel was  $A = 200 \mu\text{m} \times 65 \mu\text{m} \approx 0.013 \text{ mm}^2$ , see Fig. 2. The dielectric constant  $\varepsilon_C$  of the layer structure between the gate electrode and the field-effect channel can be approximated by the dielectric constant of GaAs ( $\approx 13.1$ ) and the permittivity  $\varepsilon_0$  is  $8.9 \times 10^{-12} \text{ Fm}^{-1}$ . This results in  $C \approx 60$  pF.  $R = R_1 R_i / (R_1 + R_i)$  is the resistance including both sides of the field-effect channel, where  $R_1$  includes the inner resistance  $R_i = 20 \text{ M}\Omega$  of the current source, see Fig. 8. Due to the voltage dependence of the channel resistance,  $R_C$  is highest at the intersection with the negatively biased gate electrode, see Fig. 4a. Therefore, the contribution of unbiased parts of the channel to the total resistance can be neglected in first order. At the working point used in this study, the resistance of the field-effect channel was about  $15 \text{ M}\Omega$ . Since this resistance cannot be unequivocally be attributed to the left or the right side of the channel,  $R$  was assumed to be  $\approx 6\text{--}15 \text{ M}\Omega$ . These numerical values yield  $RC \approx 0.36\text{--}0.9$  ms and, thus, a transition frequency  $1/2\pi RC \approx 180\text{--}440$  Hz. This result is in the same order of magnitude as the experimentally obtained transition frequency and, thus, corroborates the small-signal model described above.

In this study, a potential sensitivity of  $\delta\Phi \approx 150 \mu\text{V}$  was obtained at the working point of the described test structure at a time resolution of 3 kHz. This first FAPS test structure was based on a commercially available heterostructure, which was not optimized for this purpose. Therefore, it should be possible to further improve the potential sensitivity, e.g. by using a heterostructure with more mobile electrons and therefore a lower channel resistance for gate voltages around zero, and a current source with higher input resistance.

However, in order to design a FAPS detector with many active sites, the dimension of the field-effect channels and gate electrodes has to be reduced. By using the equivalent circuit shown in Fig. 8, it will be discussed in the following, whether scaling down of the geometrical arrangement has an effect on the potential sensitivity. At given time resolution  $\omega_{\text{MOD}}$ , the voltage sensitivity is mainly limited by the collapse of the slope of the transfer characteristics  $dU_C/dU_B(\omega_{\text{MOD}})$ , see Fig. 6b. The transition frequency of the onset of the decay of the slope is given by the value of  $RC$ . If both the width of the field-effect channels and the gate electrodes would be reduced by half,  $C$  would be reduced by a factor 4, since it is proportional to the area of the cross-section of one channel and one gate. In contrast, in crude approximation,  $R$  would remain constant since it is proportional to the width of one channel as well as to the reciprocal length of the depleted region, which is determined by the width of one gate electrode. Altogether, in this approximation,  $RC$  would be reduced by a factor of 4 and, therefore, the onset of the collapse in the slope would be shifted to the fourfold frequency. Therefore, the potential sensitivity at high frequencies should be im-

proved if the FAPS-structure is scaled down to smaller arrangements.

In this way, the potential sensitivity of the FAPS and FET arrays can be compared. The transfer characteristics of a FET is given by its voltage-dependent drain-source current  $I_{\text{DS}}(U_{\text{B}})$ . Under working conditions, for example, the FETs described by the group of Offenhäusser have a quasi-static slope of  $dI_{\text{DS}}/dU_{\text{B}} \approx 0.1\text{--}0.4 \text{ k}\Omega^{-1}$  and the noise in current measurements after a 3 kHz low-pass filter is  $\delta I_{\text{DS}} \approx 10 \text{ nA}$  [7,16,17].  $R$  can be assumed as the resistance of the drain-source channel and was reported to be  $R = (dI_{\text{DS}}/dU_{\text{B}})^{-1} \approx 2\text{--}10 \text{ M}\Omega$ . The size of one gate  $A$  of the described FETs was between  $10 \times 4$  and  $28 \times 12 \mu\text{m}$  and, thus,  $\approx 40\text{--}340 \mu\text{m}^2$ . The thickness of the gate oxide was  $d \approx 10 \text{ nm}$  and the dielectric constant of  $\text{SiO}_2$  is  $\varepsilon_G \approx 3.6$ . This yields a capacitance  $C = \varepsilon_0 \varepsilon_G A/d \approx 0.15\text{--}1 \text{ pF}$  and, thus,  $RC \approx 0.3\text{--}10 \text{ ns}$ . Therefore, the transition frequency  $(2\pi RC)^{-1} \approx 15\text{--}50 \text{ MHz}$  is shifted to very high frequencies and time resolution of 3 kHz can be described as quasi-static state. Hence, the potential sensitivity at a time resolution of 3 kHz of the FETs described here is  $\delta\Phi = \delta I_{\text{DS}}/(dI_{\text{DS}}/dU_{\text{B}}) \approx 25\text{--}100 \mu\text{V}$  and is, therefore, up to one order of magnitude better than the voltage sensitivity that has been obtained with the FAPS test structure in this study [7,16]. The potential sensitivity of a FAPS test structure with comparable extensions can be estimated by assuming a width of  $6\text{--}18 \mu\text{m}$  of both field-effect channels and gate electrodes. The area of one cross-section would be  $A \approx 40\text{--}320 \mu\text{m}^2$  and, thus,  $C \approx 0.2\text{--}1.5 \text{ pF}$ ,  $R \approx 6\text{--}15 \text{ M}\Omega$  and  $RC \approx 1.2\text{--}22 \mu\text{s}$ . The transition frequency would be  $(2\pi RC)^{-1} \approx 7\text{--}130 \text{ kHz}$  and, hence, a time resolution of 3 kHz could be described as quasi-static state. According to this model, the potential sensitivity of such a FAPS structure would be  $\delta\Phi = \delta U_C/(dU_C/dU_{\text{B}}) = 65 \mu\text{V}/22 \approx 3 \mu\text{V}$  and, therefore, even better than that of the FETs described above. In regard of the crude approximations on which this model is based, this quantitative value can only be interpreted as rough estimation. However, the analysis suggests that by scaling down the size of the field-effect channels and the gate electrodes, a FAPS device with a potential sensitivity better than a few  $10 \mu\text{V}$  should be possible.

In the model analysis presented in this study, it has been shown that the potential sensitivity of a test structure, which consists of one field-effect channel and one gate electrode, is improved if the widths of the channel and the gate are reduced. For a sensor with spatial resolution, many sites are needed. If the number of field-effect channels and gate electrodes is increased to design a highly integrated device, however, the length of the field-effect channels and, thus,  $R$  will increase. This suggests that a gain in the number of active sites has to be paid by a loss in the potential sensitivity.

To corroborate the predictions for a scaled down FAPS in the next future step, a small test structure with 10 field-effect channels with a width and a spacing of  $\approx 10$

$\mu\text{m}$ , and 10 gate electrodes with a width and a spacing of  $\approx 10 \mu\text{m}$  and, thus,  $10 \times 10$  sites will be developed. Because of its geometric properties, the potential sensitivity of such a device should be better than the test structure that has been discussed in this report. In addition, with such a highly integrated structure, the option of spatial resolution of the FAPS could be tested by applying test potentials from above at different sites, e.g. by using microelectrodes.

Furthermore, future devices have to be tested in electrolytic solution, i.e. with a drop of electrolyte on top of the structure. Under such conditions, the whole front side of the device will be biased at a constant offset potential due to the high conductivity of the electrolyte. However, potential fluctuations located above individual intersections of field-effect channels and backgate electrodes add to this offset potential and should change the channel resistance and, therefore, are likely to be detectable. This is very similar to the concept of FET arrays in which multiple gate electrodes are covered by a drop of electrolyte and the electric contact is generated with one single reference electrode [4,16]. Therefore, the FAPS should be well suited to detect surface potentials spatially resolved in electrolytic solution, although the experimental proof remains a topic of a future study.

### Acknowledgements

The authors are grateful to Prof. J.P. Kotthaus for helpful discussions and comments, and to Siemens, München, for providing the semiconductor substrates.

### References

- [1] W. Göpel, Chemical imaging: I. Concepts and visions for electronic and bioelectronic noses, *Sens. Actuators, B* 52 (1998) 125–142.

- [2] U. Weimar, W. Göpel, Chemical imaging: II. Trends in practical multiparameter sensor systems, *Sens. Actuators, B* 52 (1998) 143–161.
- [3] P. Bergveld, The development and application of FET-based biosensors, *Biosensors* 2 (1986) 15–33.
- [4] I. Igarashi, T. Ito, T. Taguchi, O. Tabata, H. Inagaki, Multiple ion sensor array, *Sens. Actuators, B:Chemical* 1 (1990) 8–11.
- [5] B.H.v.d. Schoot, P. Bergveld, ISFET based enzyme sensors, *Biosensors* 3 (1987) 161–186.
- [6] R. Weis, B. Müller, P. Fromherz, Neuron adhesion on a silicon chip probed by an array of field-effect transistors, *Phys. Rev. Lett.* 76 (1996) 327–330.
- [7] C. Sprössler, D. Richter, M. Denyer, A. Offenhäusser, Long-term recording system based on field-effect transistor arrays for monitoring electrogenic cells in culture, *Biosens. Bioelectron.* 13 (1998) 613–618.
- [8] W.J. Parak, M. George, H.E. Gaub, S. Böhm, A. Lorke, The field-effect-addressable potentiometric sensor/stimulator (FAPS) — a new concept for a surface potential sensor and stimulator with spatial resolution, *Sens. Actuators, B* 58 (1999) 497–504.
- [9] T. Ando, A.B. Fowler, F. Stern, Electronic properties of two-dimensional systems, *Rev. Mod. Phys.* 54 (1982) 437–672.
- [10] P. Bergveld, J. Wiersma, H. Meertens, Extracellular potential recordings by means of a field effect transistor without gate metal, called OSFET, *IEEE Trans. Biomed. Eng.* 23 (1976) 136–144.
- [11] P. Fromherz, A. Offenhäusser, T. Vetter, J. Weis, A neuron-silicon junction: a Retzius cell of the leech on an insulated-gate field-effect transistor, *Science* 252 (1991) 1290–1293.
- [12] M. Grattarola, G. Massobrio, P. Antognetti, *Bioelectronics Handbook: MOSFETs, Biosensors, and Neurons*, McGraw-Hill, New York, 1998.
- [13] E. Yablonovitch, T. Gmitter, J.P. Harbison, R. Bhat, Extreme selectivity in the lift-off of epitaxial GaAs films, *Appl. Phys. Lett.* 51 (1987) 2222–2224.
- [14] E. Yablonovitch, D.M. Hwang, T.J. Gmitter, I.T. Florez, J.P. Harbison, Van der Waals bonding of GaAs epitaxial lift-off films onto arbitrary substrates, *Appl. Phys. Lett.* 56 (1990) 2419–2421.
- [15] S.M. Sze, *VSLI Technology*, McGraw-Hill, New York, 1988.
- [16] C. Sprössler, M. Denyer, S. Britland, W. Knoll, A. Offenhäusser, Electrical recordings from rat cardiac muscle cells using field-effect transistors, *Phys. Rev. E* 60 (1999) 2171–2176.
- [17] A. Offenhäusser, C. Sprössler, M. Matsuzawa, W. Knoll, Field-effect transistor array for monitoring electrical activity from mammalian neurons in culture, *Biosens. Bioelectron.* 12 (1997) 819–826.